Acta Mech. Sin. (2012) 28(1):83–90
10.1007/s10409-011-0546-5

RESEARCH PAPER

Axisymmetric compressive buckling of multi-walled carbon nanotubes under different boundary conditions

Cheng-Qi Sun · Kai-Xin Liu · You-Shi Hong

Received: 27 August 2010 / Revised: 13 June 2011 / Accepted: 5 September 2011

Abstract The paper studies the axisymmetric compressive buckling behavior of multi-walled carbon nanotubes (MWNTs) under different boundary conditions based on continuum mechanics model. A buckling condition is derived for determining the critical buckling load and associated buckling mode of MWNTs, and numerical results are worked out for MWNTs with different aspect ratios under fixed and simply supported boundary conditions. It is shown that the critical buckling load of MWNTs is insensitive to boundary conditions, except for nanotubes with smaller radii and very small aspect ratio. The associated buckling modes for different layers of MWNTs are in-phase, and the buckling displacement ratios for different layers are independent of the boundary conditions and the length of MWNTs. Moreover, for simply supported boundary conditions, the critical buckling load is compared with the corresponding one for axial compressive buckling, which indicates that the critical buckling load for axial compressive buckling can be well approximated by the corresponding one for axisymmetric compressive buckling. In particular, for axial compressive buckling of double-walled carbon nanotubes, an analytical expression is given for approximating the critical buckling load. The present investigation may be of some help in further understanding the mechanical properties of MWNTs.

Keywords Carbon nanotube · Buckling · van der Waals forces

The project was supported by the National Natural Science Foundation of China (10721202, 10732010, 10972010 and 11028206).

C. Sun (✉) · Y. Hong
The State Key Laboratory of Nonlinear Mechanics,
Institute of Mechanics, Chinese Academy of Sciences,
100190 Beijing, China
e-mail: scq@lnm.imech.ac.cn

K. Liu
LTCS and Department of Mechanics & Aerospace Engineering,
College of Engineering, Peking University,
100871 Beijing, China

1 Introduction

Since the discovery of carbon nanotubes (CNTs), the mechanical behaviors of single-walled carbon nanotube (SWNT) or MWNTs have been widely investigated by employing experiments, continuum mechanics model, and molecular dynamic simulations [1–5]. For example, Yakobson et al. [6] compared the results of atomistic modeling for axial compressive buckling of SWNTs with a continuum shell model and found that the continuum shell model could well predict all the changes of buckling patterns displayed by the molecular dynamics simulations. Ru [7, 8] presented an elastic double-shell model for studying axial compressive buckling of a DWNT and a DWNT in an elastic medium. In Ru's analysis, the effect of van der Waals forces was included and an approximate linear relation was adopted to model the van der Waals interaction between intertube. Han and Lu [9] presented an elastic double-shell model for the torsional buckling of an embedded DWNT, and showed that inserting an inner nanotube into an embedded single-walled one would reduce the critical buckling load of the initially embedded SWNT under otherwise identical conditions. Liu et al. [10] investigated the effect of bending instabilities on the measurements of mechanical properties of MWNTs based on the theory of finite elasticity. It was shown that the rippling mode was permissible by the nonlinear theory, and that the dependence of the bending moment on the bending curvature could be approximated by a bilinear constitutive relation. In their results, it was indicated that, in

some mechanical properties of CNTs from measurements, one needs to be particularly cautious in using classical results obtained from the linear elasticity. Wang et al. [11, 12] studied elastic buckling of individual MWNTs under external radial pressure and axially compressed buckling of pressured MWNTs using a multiple-shell model. Their results showed that the predicted critical pressure and the predicted increment of critical axial stress due to an internal radial pressure using continuum mechanics model were in reasonably good agreement with the experiment results [13] and the results for filled CNTs by molecular dynamics simulations [14], respectively. Wang et al. [15] studied the effect of van der Waals forces on the pull-in stability of CNTs using the cantilever beam with large deformation model. Wang et al. [16] studied the size dependence of thin-shell model for CNTs and showed that the size dependence is insignificant for SWNTs of diameters larger than 1.5 nm. In their analysis, it was indicated that, for SWNTs with diameter larger than about 1.5 nm, an isotropic thin-shell model with constant thickness and elastic moduli could be used. Akita et al. [17] studied the buckling of MWNTs under axial compression and showed that the molecular dynamics simulations for buckling behavior of triple- and double-walled CNTs were consistent with the continuum analysis. Xie et al. [18] investigated the effect of small size-scale on radial buckling pressure of a simply supported MWNT based on the theory of nonlocal continuum mechanics. Sun et al. [19, 20] studied dynamic buckling behavior of MWNTs under axial impact load and impact torque based on continuum mechanics model, and derived a buckling condition for determining the buckling load and associated buckling mode by introducing the initial imperfections for MWNTs and applying the method of preferred mode.

Many researches have shown that continuum mechanics model can capture the main factor affecting mechanical behaviors of CNTs and can be an effective method to study the mechanical behaviors of CNTs even for CNTs with very small radius [21–24]. Especially, due to the difficulty of experiment at nanoscale and the limitation of molecular dynamics simulation for very large atomic system, continuum mechanics model has been widely used to investigate mechanical behaviors of MWNTs or DWNTs in various environments [25–27].

However, to the authors' knowledge, the effect of boundary conditions on the buckling behavior of MWNTs has been an open topic. Actually, MWNTs are always subjected to different boundary conditions in their potential applications as basic elements of nanoscale devices, and the effect of boundary conditions can not be neglected in certain circumstances. Motivated by these considerations, the paper reports a method for studying axisymmetric compressive buckling behavior of MWNTs under different boundary conditions based on continuum mechanics model. As examples, numerical results are worked out for DWNTs and five-layer MWNTs under fixed and simply supported boundary conditions. As a result, the effect of boundary conditions on the critical buckling load of MWNTs is revealed, and the associated buckling modes are also illustrated. Moreover, the critical buckling load under simply supported boundary condition is compared with the corresponding one for axial compressive buckling. The effect of radii is also examined.

2 Buckling analysis

2.1 Basic equations

Figure 1 shows the model of an MWNT of length L. Subscripts 1, 2, $\cdots$, N denote the corresponding quantities related to the innermost tube, its adjacent tube, $\cdots$, and the outermost tube, respectively. For MWNTs, the van der Waals interaction pressures (per unit area) between the k-th tube and the $(k+1)$-th tube are equal and opposite. Thus, the (inward) pressure exerted on the k-th tube due to the $(k+1)$-th tube, $p_{k(k+1)}$, and the similar (inward) pressure exerted on the $(k+1)$-th tube due to the k-th tube, $p_{(k+1)k}$, can be related by [11, 12]

$$p_{k(k+1)} = -\frac{R_{k+1}}{R_k} p_{(k+1)k}, \qquad k = 1, 2, \cdots, N-1, \tag{1}$$

where R_k denotes the radius of the k-th tube.

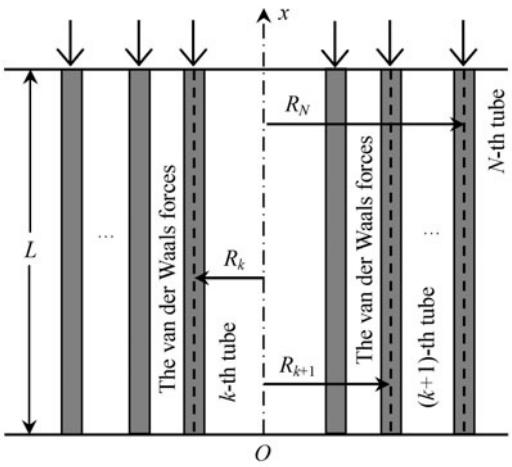

Fig. 1 Model of an MWNT of length L

In this paper, as that used by Ru [7, 8] and Wang et al. [11, 12], a linearized analysis is adopted to model the effect of van der Waals forces between intertube, i.e., the pressure $p_{k(k+1)}$ due to buckling can be described by

$$\begin{aligned} p_{12} &= c(w_2 - w_1), \\ p_{23} &= c(w_3 - w_2), \\ &\cdots, \\ p_{(N-1)N} &= c(w_N - w_{N-1}), \end{aligned} \tag{2}$$

where c is a constant determined by the slope of the van der Waals law at the initial unbuckled interlayer spacing and is estimated as $3.2\times10^{-5}\,\mathrm{J\cdot cm^{-2}}/0.16s^2$ [28], in which $s = 0.142\,\mathrm{nm}$.

The axisymmetric compressive buckling equation for an elastic shell is

$$D\frac{\mathrm{d}^4w}{\mathrm{d}x^4} - N_x^0\frac{\mathrm{d}^2w}{\mathrm{d}x^2} + \frac{Eh}{R^2}w - p = 0, \tag{3}$$

where w is an additional radial displacement of the middle surface due to buckling, x denotes axial direction, D is bending stiffness, E is Young's modulus, h is thickness, R is radius, N_x^0 is the uniform axial membrane force per unit length prior to buckling, and p is the net (inward) normal pressure.

Applying Eqs. (1)–(3) to each tube of an N-layer MWNT, N coupled equations is obtained as

$$\begin{aligned}
&D_1\frac{\mathrm{d}^4w_1}{\mathrm{d}x^4} - N_{x1}^0\frac{\mathrm{d}^2w_1}{\mathrm{d}x^2} + \frac{Eh_1}{R_1^2}w_1 - c(w_2 - w_1) = 0,\\
&D_k\frac{\mathrm{d}^4w_k}{\mathrm{d}x^4} - N_{xk}^0\frac{\mathrm{d}^2w_k}{\mathrm{d}x^2} + \frac{Eh_k}{R_k^2}w_k\\
&\qquad -c(w_{k+1} - w_k) + \frac{R_{k-1}}{R_k}c(w_k - w_{k-1}) = 0,\\
&\qquad k = 2, 3, \cdots, N-1,\\
&D_N\frac{\mathrm{d}^4w_N}{\mathrm{d}x^4} - N_{xN}^0\frac{\mathrm{d}^2w_N}{\mathrm{d}x^2} + \frac{Eh_N}{R_N^2}w_N\\
&\qquad +c\frac{R_{N-1}}{R_N}(w_N - w_{N-1}) = 0,
\end{aligned} \tag{4}$$

where D_k denotes the effective bending stiffness, and h_k denotes the effective thickness of the k-th tube.

It is seen from Eq. (4) that, for axisymmetric compressive buckling of MWNTs, it is only necessary to know the values of the effective bending stiffness D_k and the in-plane stiffness Eh_k, where $k = 1, 2, \cdots, N$. Here, we take $D_1 = D_2 = \cdots = D_N = D = 0.85\,\mathrm{eV}$, $Eh_1 = Eh_2 = \cdots = Eh_N = Eh = 360\,\mathrm{J/m^2}$ [6, 12, 23].

2.2 Buckling condition

The general solution for Eq. (4) is expressed as

$$w_k = U_k\mathrm{e}^{\lambda x}, \qquad k = 1, 2, \cdots, N, \tag{5}$$

where U_k is real constant.

With N_x denoting the applied axial compressive load, substituting Eq. (5) into Eq. (4), yields N homogeneous linear equations for $U_1, U_2, \cdots, U_N$

$$\begin{aligned}
&a_{11}U_1 + a_{12}U_2 = 0,\\
&a_{k(k-1)}U_{k-1} + a_{kk}U_k + a_{k(k+1)}U_{k+1} = 0,\\
&\qquad k = 2, 3, \cdots, N-1,\\
&a_{N(N-1)}U_{N-1} + a_{NN}U_N = 0,
\end{aligned} \tag{6}$$

where

$$\begin{aligned}
a_{11} &= D\lambda^4 + N_x\lambda^2 + \Big(c + \frac{Eh}{R_1^2}\Big),\\
a_{12} &= -c,\\
a_{k(k-1)} &= -c\frac{R_{k-1}}{R_k},\\
a_{kk} &= D\lambda^4 + N_x\lambda^2 + \Big(c\frac{R_{k-1}}{R_k} + c + \frac{Eh}{R_k^2}\Big),\\
a_{k(k+1)} &= -c,\\
a_{N(N-1)} &= -c\frac{R_{N-1}}{R_N},\\
a_{NN} &= D\lambda^4 + N_x\lambda^2 + \Big(c\frac{R_{N-1}}{R_N} + \frac{Eh}{R_N^2}\Big).
\end{aligned}$$

The requirement that Eq. (6) have non-zero solution on U_k ($k = 1, 2, \cdots, N$) gives

$$\det\boldsymbol{Q} = 0, \tag{7}$$

where $\boldsymbol{Q}$ denotes the coefficient matrix on $U_1, U_2, \cdots, U_N$.

Equation (7) contains $4N$ eigenvalue ($\lambda_1, \lambda_2, \cdots, \lambda_{4N}$) with respect to the applied axial load N_x for an N-layer MWNT. For a given eigenvalue λ_j ($j = 1, 2, \cdots, 4N$), the corresponding buckling displacement w_k is determined by Eq. (5). Thus, the buckling displacement for an N-layer MWNT can be expressed as

$$w_1 = \sum_{j=1}^{4N} A_j\mathrm{e}^{\lambda_j x}, \quad w_k = \sum_{j=1}^{4N} U_k^j A_j\mathrm{e}^{\lambda_j x}, \quad k = 2, 3, \cdots, N, \tag{8}$$

where A_j and U_k^j ($j = 1, 2, \cdots, 4N$) are constants.

As a special case ($N = 2$), an analytical expression for the buckling displacements is solved as follows.

Note that

$$\begin{aligned}
X_1 &= -\frac{1}{2}\Big(\frac{Eh}{R_1^2} + c + \frac{Eh}{R_2^2} + \frac{cR_1}{R_2}\Big)\\
&\quad + \frac{1}{2}\sqrt{\Big(\frac{Eh}{R_1^2} + c - \frac{Eh}{R_2^2} - \frac{cR_1}{R_2}\Big)^2 + 4\frac{c^2R_1}{R_2}},\\
X_2 &= -\frac{1}{2}\Big(\frac{Eh}{R_1^2} + c + \frac{Eh}{R_2^2} + \frac{cR_1}{R_2}\Big)\\
&\quad - \frac{1}{2}\sqrt{\Big(\frac{Eh}{R_1^2} + c - \frac{Eh}{R_2^2} - \frac{cR_1}{R_2}\Big)^2 + 4\frac{c^2R_1}{R_2}},\\
p &= \frac{1}{c}\Big(X_1 + \frac{Eh}{R_1^2} + c\Big),\\
q &= \frac{1}{c}\Big(X_2 + \frac{Eh}{R_1^2} + c\Big),\\
\alpha_1 &= \sqrt{\frac{N_x - \sqrt{N_x^2 + 4DX_1}}{2D}},
\end{aligned}$$

$$\alpha_2 = \sqrt{\frac{N_x + \sqrt{N_x^2 + 4DX_1}}{2D}},$$

$$\beta_1 = \sqrt{\frac{N_x - \sqrt{N_x^2 + 4DX_2}}{2D}},$$

$$\beta_2 = \sqrt{\frac{N_x + \sqrt{N_x^2 + 4DX_2}}{2D}},$$

$$\gamma_1 = \frac{\sqrt{-N_x + 2\sqrt{-DX_1}}}{2\sqrt{D}},$$

$$\gamma_2 = \frac{\sqrt{N_x + 2\sqrt{-DX_1}}}{2\sqrt{D}},$$

$$\kappa_1 = \frac{\sqrt{-N_x + 2\sqrt{-DX_2}}}{2\sqrt{D}},$$

$$\kappa_2 = \frac{\sqrt{N_x + 2\sqrt{-DX_2}}}{2\sqrt{D}}.$$

Case 1: $N_x^2 + 4DX_2 > 0$

$$\begin{aligned} w_1 &= A_1\cos\alpha_1 x + A_2\sin\alpha_1 x + A_3\cos\alpha_2 x \\ &\quad + A_4\sin\alpha_2 x + A_5\cos\beta_1 x + A_6\sin\beta_1 x \\ &\quad + A_7\cos\beta_2 x + A_8\sin\beta_2 x, \end{aligned} \tag{9}$$

$$\begin{aligned} w_2 &= A_1 p\cos\alpha_1 x + A_2 p\sin\alpha_1 x + A_3 p\cos\alpha_2 x \\ &\quad + A_4 p\sin\alpha_2 x + A_5 q\cos\beta_1 x + A_6 q\sin\beta_1 x \\ &\quad + A_7 q\cos\beta_2 x + A_8 q\sin\beta_2 x. \end{aligned} \tag{10}$$

Case 2: $N_x^2 + 4DX_2 = 0$

$$\begin{aligned} w_1 &= A_1\cos\alpha_1 x + A_2\sin\alpha_1 x + A_3\cos\alpha_2 x \\ &\quad + A_4\sin\alpha_2 x + (A_5 + A_6 x)\cos\sqrt{-\frac{X_2}{D}}x \\ &\quad + (A_7 + A_8 x)\sin\sqrt{-\frac{X_2}{D}}x, \end{aligned} \tag{11}$$

$$\begin{aligned} w_2 &= A_1 p\cos\alpha_1 x + A_2 p\sin\alpha_1 x + A_3 p\cos\alpha_2 x \\ &\quad + A_4 p\sin\alpha_2 x + (A_5 + A_6 x)q\cos\sqrt{-\frac{X_2}{D}}x \\ &\quad + (A_7 + A_8 x)q\sin\sqrt{-\frac{X_2}{D}}x. \end{aligned} \tag{12}$$

Case 3: $N_x^2 + 4DX_2 < 0 < N_x^2 + 4DX_1$

$$\begin{aligned} w_1 &= A_1\cos\alpha_1 x + A_2\sin\alpha_1 x + A_3\cos\alpha_2 x \\ &\quad + A_4\sin\alpha_2 x + A_5 e^{\kappa_1 x}\cos\kappa_2 x + A_6 e^{\kappa_1 x}\sin\kappa_2 x \\ &\quad + A_7 e^{-\kappa_1 x}\cos\kappa_2 x + A_8 e^{-\kappa_1 x}\sin\kappa_2 x, \end{aligned} \tag{13}$$

$$\begin{aligned} w_2 &= A_1 p\cos\alpha_1 x + A_2 p\sin\alpha_1 x + A_3 p\cos\alpha_2 x \\ &\quad + A_4 p\sin\alpha_2 x + A_5 q e^{\kappa_1 x}\cos\kappa_2 x + A_6 q e^{\kappa_1 x}\sin\kappa_2 x \\ &\quad + A_7 q e^{-\kappa_1 x}\cos\kappa_2 x + A_8 q e^{-\kappa_1 x}\sin\kappa_2 x. \end{aligned} \tag{14}$$

Case 4: $N_x^2 + 4DX_1 = 0$

$$\begin{aligned} w_1 &= (A_1 + A_2 x)\cos\sqrt{-\frac{X_1}{D}}x + (A_3 + A_4 x)\sin\sqrt{-\frac{X_1}{D}}x \\ &\quad + A_5 e^{\kappa_1 x}\cos\kappa_2 x + A_6 e^{\kappa_1 x}\sin\kappa_2 x \\ &\quad + A_7 e^{-\kappa_1 x}\cos\kappa_2 x + A_8 e^{-\kappa_1 x}\sin\kappa_2 x, \end{aligned} \tag{15}$$

$$\begin{aligned} w_2 &= (A_1 + A_2 x)p\cos\sqrt{-\frac{X_1}{D}}x + (A_3 + A_4 x)p\sin\sqrt{-\frac{X_1}{D}}x \\ &\quad + A_5 p e^{\kappa_1 x}\cos\kappa_2 x + A_6 q e^{\kappa_1 x}\sin\kappa_2 x \\ &\quad + A_7 q e^{-\kappa_1 x}\cos\kappa_2 x + A_8 q e^{-\kappa_1 x}\sin\kappa_2 x. \end{aligned} \tag{16}$$

Case 5: $N_x^2 + 4DX_1 < 0$

$$\begin{aligned} w_1 &= A_1 e^{\gamma_1 x}\cos\gamma_2 x + A_2 e^{\gamma_1 x}\sin\gamma_2 x + A_3 e^{-\gamma_1 x}\cos\gamma_2 x \\ &\quad + A_4 e^{-\gamma_1 x}\sin\gamma_2 x + A_5 e^{\kappa_1 x}\cos\kappa_2 x + A_6 e^{\kappa_1 x}\sin\kappa_2 x \\ &\quad + A_7 e^{-\kappa_1 x}\cos\kappa_2 x + A_8 e^{-\kappa_1 x}\sin\kappa_2 x, \end{aligned} \tag{17}$$

$$\begin{aligned} w_2 &= A_1 p e^{\gamma_1 x}\cos\gamma_2 x + A_2 p e^{\gamma_1 x}\sin\gamma_2 x + A_3 p e^{-\gamma_1 x}\cos\gamma_2 x \\ &\quad + A_4 p e^{-\gamma_1 x}\sin\gamma_2 x + A_5 q e^{\kappa_1 x}\cos\kappa_2 x + A_6 q e^{\kappa_1 x}\sin\kappa_2 x \\ &\quad + A_7 q e^{-\kappa_1 x}\cos\kappa_2 x + A_8 q e^{-\kappa_1 x}\sin\kappa_2 x. \end{aligned} \tag{18}$$

In this paper, we only consider the following two important boundary conditions.

(1) The fixed boundary conditions

$$w_k = \frac{\partial w_k}{\partial x} = 0, \quad k = 1, 2, \cdots, N, \quad \text{at } x = 0 \text{ and } x = L. \tag{19}$$

(2) The simply supported boundary conditions

$$w_k = \frac{\partial^2 w_k}{\partial x^2} = 0, \quad k = 1, 2, \cdots, N, \quad \text{at } x = 0 \text{ and } x = L. \tag{20}$$

By making use of the boundary conditions Eq. (19) or Eq. (20), $4N$ homogeneous linear equations are obtained on $A_1, A_2, \cdots, A_{4N}$, i.e.,

$$\boldsymbol{M}\cdot\boldsymbol{A} = \boldsymbol{0}, \tag{21}$$

where $\boldsymbol{M}$ is the coefficient matrix on $A_1, A_2, \cdots, A_{4N}$, and $\boldsymbol{A} = [A_1, A_2, \cdots, A_{4N}]^{\mathrm{T}}$.

The non-zero solution of Eq. (21) provides the buckling condition, i.e.,

$$\det\boldsymbol{M} = 0. \tag{22}$$

From Eq. (22), the critical buckling load N_{cr} (the minimum axial load N_x) can be determined with the associated buckling mode obtained.

3 Numerical results and discussion

3.1 Axisymmetric compressive buckling of DWNTs and five-layer MWNTs

Figure 2 shows dimensionless critical buckling load $N_{cr}/(-4DX_1)^{1/2}$ versus inner radius for DWNTs under fixed and simply supported boundary conditions, for four different values of aspect ratio $L/R_2 = 1, 2, 5, 12$, respectively. Similar plots, but for five-layer MWNTs, are given in Fig. 3, where X_1' denotes the corresponding largest negative root on $D\lambda^4 + N_x\lambda^2$ obtained from Eq. (7). It is seen from Figs. 2 and 3 that, the effect of boundary conditions on the critical buckling load of MWNTs is related to the radii and aspect ratio, which is big for MWNTs with inner/innermost radius of about several nanometers and very small aspect ratio. For example, the critical buckling load for DWNT with inner radius $R_1 = 1$ nm and aspect ratio $L/R_2 = 1$ under fixed boundary conditions is up to about 23% larger than the one under simply supported boundary conditions under otherwise identical conditions. While for MWNTs with large radii or big aspect ratio, the effect of boundary conditions on the critical buckling load is usually very small and can be negligible.

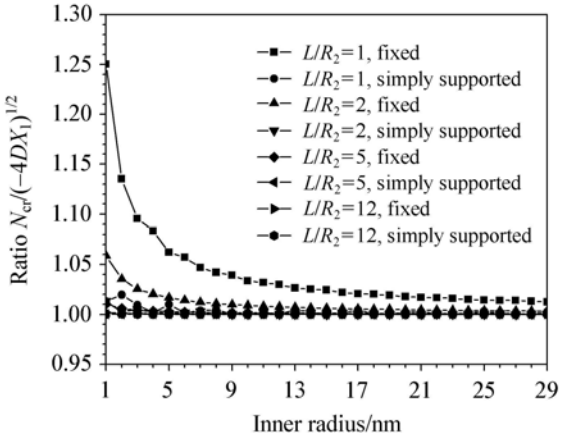

Fig. 2 Plot of $N_{cr}/(-4DX_1)^{1/2}$ versus inner radius for DWNTs under fixed and simply supported boundary conditions, at $L/R_2 = 1$, 2, 5 and 12, respectively

Figures 2 and 3 also indicate that, for large values of aspect ratio (such as larger than 2), the value $(-4DX_1)^{1/2}$ and $(-4DX_1')^{1/2}$ are very close to the critical buckling load of DWNTs and that of five-layer MWNTs, respectively. As seen in Figs. 2 and 3, with R_1 ranging from 1 nm to 29 nm, the relative error of $(-4DX_1)^{1/2}$ or $(-4DX_1')^{1/2}$ over the critical buckling load of DWNTs or five-layer MWNTs is less than 6% or 3.5% for all the three values of aspect ratios 2, 5 and 12. This indicates that, for axisymmetric compressive buckling of MWNTs with large radii or big aspect ratio, the critical buckling load can be well approximated by the value $(-4DX)^{1/2}$, where X denotes the biggest negative root on $D\lambda^4 + N_x\lambda^2$ obtained from Eq. (7). In particular, for axisymmetric compressive buckling of DWNTs, an explicit expression is obtained, i.e.

$$N_{cr} \approx \left[2D\left(\frac{Eh}{R_1^2} + c + \frac{Eh}{R_2^2} + \frac{cR_1}{R_2}\right) - 2D\sqrt{\left(\frac{Eh}{R_1^2} + c - \frac{Eh}{R_2^2} - \frac{cR_1}{R_2}\right)^2 + 4\frac{c^2R_1}{R_2}}\right]^{1/2}.$$

Figures 4 and 5 show associated buckling displacement ratio of different layers versus inner/innermost radius for the DWNTs and the five-layer MWNTs referred in Figs. 2 and 3. It is seen that, for both the DWNTs and the five-layer MWNTs, the associated buckling modes for different layers are in-phase, and the displacement ratios for different layers are independent of the boundary conditions, and independent of the length of CNTs. However, the associated buckling displacement ratios are related to the radii of MWNTs, which increase with increasing inner/innermost radius of MWNTs.

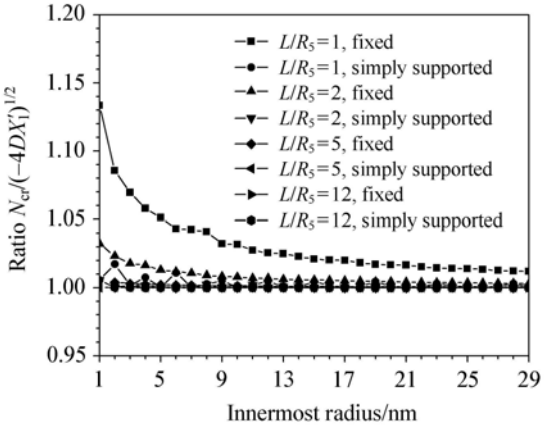

Fig. 3 Plot of $N_{cr}/(-4DX_1')^{1/2}$versus innermost radius for five-layer MWNTs under fixed and simply supported boundary conditions, at $L/R_5 = 1$, 2, 5 and 12, respectively

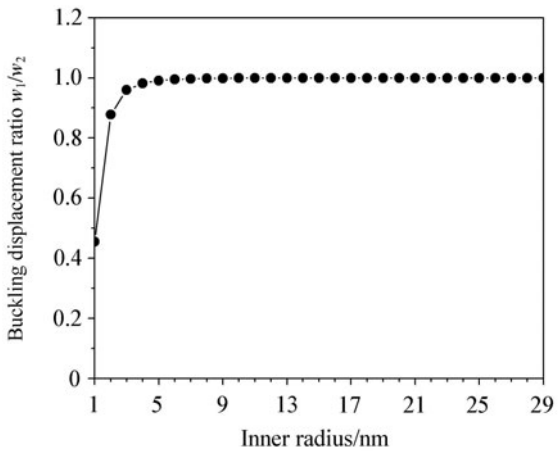

Fig. 4 Associated buckling displacement ratio w_1/w_2 versus inner radius for the DWNTs studied in Fig. 2

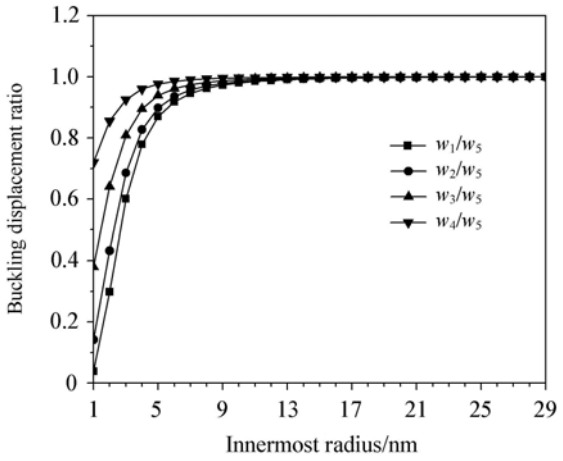

Fig. 5 Associated buckling displacement ratio of different layers versus innermost radius for the five-layer MWNTs studied in Fig. 3

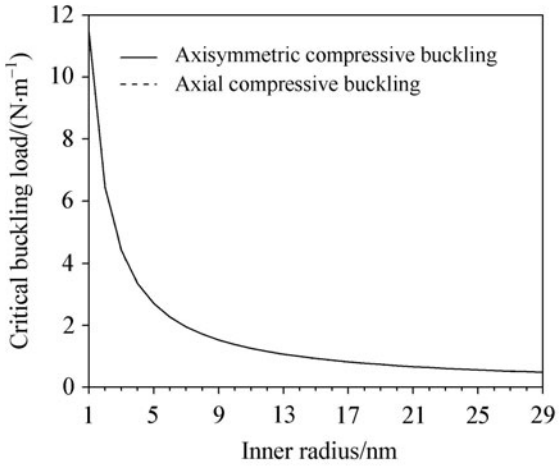

Fig. 6 Dependence of critical buckling load on inner radius for axial compressive buckling and axisymmetric compressive buckling of DWNTs at $L/R_2 = 12$

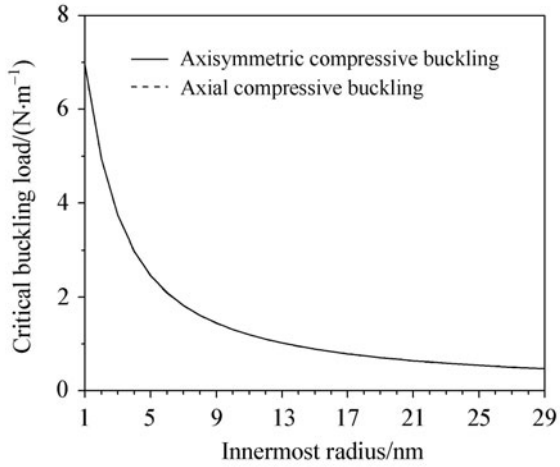

Fig. 7 Dependence of critical buckling load on innermost radius for axial compressive buckling and axisymmetric compressive buckling of five-layer MWNTs at $L/R_5 = 12$

For MWNTs with large inner/innermost radius (bigger than around 5 nm for DWNTs in Fig. 4, or bigger than around 10 nm for MWNTs in Fig. 5), the associated buckling displacements for different layers are almost the same. This indicates that, due to the effect of the van der Waals forces, the axisymmetric compressive buckling behavior of an N-layer MWNT with large innermost radius is very similar to that of a single nanotube with effective thickness Nh.

3.2 Comparison with the axial compressive buckling

It is known that, for axial compressive buckling of a long cylindrical shell under simply supported boundary condition, the critical buckling load is the same as the one for axisymmetric compressive buckling under otherwise identical conditions [29]. It will be shown in the following that this is also valid for the critical buckling load of MWNTs for axial compressive buckling, i.e., the critical buckling load of MWNTs for axial compressive buckling can be well approximated by the corresponding one for axisymmetric compressive buckling.

Figures 6 and 7 show, respectively, the critical buckling load versus inner/innermost radius for axisymmetric compressive buckling of DWNTs and five-layer MWNTs subjected to simply supported boundary condition, with a comparison to the corresponding critical buckling load for axial compressive buckling calculated from the model presented in Ref. [12]. It can be seen that, for both DWNTs and five-layer MWNTs, the critical buckling load for axial compressive buckling and the one for axisymmetric compressive buckling are very close to each other, and have the same trend of variation versus the inner/innermost radius. With the increase of inner/innermost radius, they both decrease very sharply in the initial stage.

Figure 8 shows relative variation of the critical buckling load for axisymmetric compressive buckling over that for axial compressive buckling, corresponding to Figs. 6 and 7, respectively. As illustrated in Fig. 8, for both the DWNTs and five-layer MWNTs, the relative variation is very small (less than 0.2%) with inner/innermost radius ranging from 1 nm to 29 nm. This indicates that the critical buckling load of MWNTs for axial compressive buckling can be well approximated by the corresponding one for axisymmetric compressive buckling.

Further, from the above analysis for axisymmetric compressive buckling behavior of DWNTs and five-layer MWNTs, it is observed that, for MWNTs with big radii or large aspect ratio, the critical buckling load for axial compressive buckling can also be well approximated by the value $(-4DX)^{1/2}$, which greatly simplifies the solution procedure. In particular, for axial compressive buckling of DWNTs, the

critical buckling load is well approximated by an analytic formula, i.e.

$$N_{\mathrm{cr}} \approx \left[2D\left(\frac{Eh}{R_1^2}+c+\frac{Eh}{R_2^2}+\frac{cR_1}{R_2}\right) -2D\sqrt{\left(\frac{Eh}{R_1^2}+c-\frac{Eh}{R_2^2}-\frac{cR_1}{R_2}\right)^2+4\frac{c^2R_1}{R_2}}\right]^{1/2}.$$

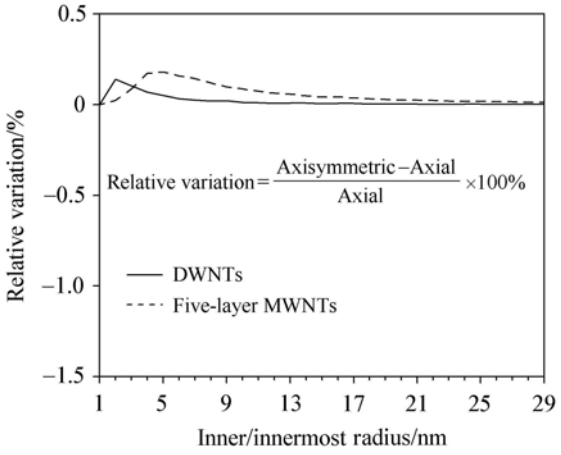

Fig. 8 Relative variation of critical buckling load for axisymmetric compressive buckling over that for axial compressive buckling, corresponding to Figs. 6 and 7, respectively

4 Conclusions

The paper presents a method for studying axisymmetric compressive buckling behavior of MWNTs under different boundary conditions based on continuum mechanics model, which takes into account the effect of the van der Waals forces between adjacent layers. A buckling condition is derived for determining the critical buckling load and associated buckling mode of MWNTs, and an analytical expression is given for the buckling displacements of DWNTs. As examples, numerical results are worked out for DWNTs and five-layer MWNTs with different aspect ratios under fixed and simply supported boundary conditions. It is shown that the effect of boundary conditions on the critical buckling load of MWNTs is related to the radii and the aspect ratio, which is very small and can be negligible except for nanotubes with smaller radii and very small aspect ratio. The associated buckling modes for different layers of MWNTs are in-phase, and the relation among the buckling displacements for different layers is independent of the boundary conditions, and independent of the length of MWNTs. Additionally, for simply supported boundary conditions, the critical buckling load for axisymmetric compressive buckling is compared with the corresponding one for axial compressive buckling. It is indicated that, for MWNTs with big radii or large aspect ratio, the critical buckling load for both axisymmetric compressive buckling and axial compressive buckling can be well approximated by the value $(-4DX)^{1/2}$, which greatly simplify the solution procedure. The result also indicates that the radii play an important role in buckling behavior of MWNTs.

References

1 Zhang, P., Huang, Y., Geubelle, P.H., et al.: On the continuum modeling of carbon nanotubes. Acta Mech. Sin. **18**(5), 528–536 (2002)

2 Guo, W.L., Guo, Y.F.: The coupled effects of mechanical deformation and electronic properties in carbon nanotubes. Acta Mech. Sin. **20**(2), 192–198 (2004)

3 Waters, J.F., Guduru, P.R., Jouzi, M., et al.: Shell buckling of individual multiwalled carbon nanotubes using nanoindentation. Appl. Phys. Lett. **87**, 103109 (2005)

4 Cao, G.X., Chen, X.: Buckling of single-walled carbon nanotubes upon bending: Molecular dynamics simulations and finite element method. Phys. Rev. B **73**, 155435 (2006)

5 Wang, Y., Fang, D.N., Soh, A.K., et al.: A molecular mechanics approach for analyzing tensile nonlinear deformation behavior of single-walled carbon nanotubes. Acta Mech. Sin. **23**(6), 663–671 (2007)

6 Yakobson, B.I., Brabec, C.J., Bernholc, J.: Nanomechanics of carbon tubes: instability beyond linear response. Phys. Rev. Lett. **76**, 2511–2514 (1996)

7 Ru, C.Q.: Effect of van der Waals forces on axial buckling of a double-walled carbon nanotube. J. Appl. Phys. **87**, 7227–7231 (2000)

8 Ru, C.Q.: Axially compressed buckling of a doublewalled carbon nanotube embedded in an elastic medium. J. Mech. Phys. Solids **49**, 1265–1279 (2001)

9 Han, Q., Lu, G.X.: Torsional buckling of a double-walled carbon nanotube embedded in an elastic medium. Eur. J. Mech. A Solids **22**, 875–883 (2003)

10 Liu, J.Z., Zheng, Q.S., Jiang, Q.: Effect of bending instabilities on the measurements of mechanical properties of multiwalled carbon nanotubes. Phys. Rev. B **67**, 075414 (2003)

11 Wang, C.Y., Ru, C.Q., Mioduchowski, A.: Elastic buckling of multiwall carbon nanotubes under high pressure. J. Nanosci. Nanotechnol. **3**, 199–208 (2003)

12 Wang, C.Y., Ru, C.Q., Mioduchowski, A.: Axially compressed buckling of pressured multiwall carbon nanotubes. Int. J. Solids Struct. **40**, 3893–3911 (2003)

13 Tang, D.S., Bao, Z.X., Wang, L.J., et al.: The electrical behavior of carbon nanotubes under high pressure. J. Phys. Chem. Solids **61**, 1175–1178 (2000)

14 Ni, B., Sinnott, S.B., Mikulski, P.T., et al.: Compression of carbon nanotubes filled with C 60, CH4, or Ne: predictions from molecular dynamics simulations. Phys. Rev. Lett. **88**, 205505 (2002)

15 Wang, G.W., Zhang, Y., Zhao, Y.P., et al.: Pull-in stability study of nanotubes under van der Waals forces influence. J. Micromech. Microeng. **14**, 1119–1125 (2004)

16 Wang, L.F., Zheng, Q.S., Liu, J.Z., et al.: Size dependence of the thin-shell model for carbon nanotubes. Phys. Rev. Lett. **95**, 105501-1–105501-4 (2005)
17 Akita, S., Nishio, M., Nakayama, Y.: Buckling of multiwall carbon nanotubes under axial compression. Jpn. J. Appl. Phys. **45**, 5586–5589 (2006)
18 Xie, G.Q., Han, X., Liu, G.R., et al.: Effect of small size-scale on the radial buckling pressure of a simply supported multi-walled carbon nanotube. Smart Mater. Struct. **15**, 1143–1149 (2006)
19 Sun, C., Liu, K., Lu, G.: Dynamic torsional buckling of multi-walled carbon nanotubes embedded in an elastic medium. Acta Mech. Sin. **24**, 541–547 (2008)
20 Sun, C., Liu, K.: Dynamic column buckling of multi-walled carbon nanotubes under axial impact load. Solid State Commun. **149**, 429–433 (2009)
21 Yakobson, B.I., Smalley, R.E.: Fullerene nanotubes: C-1000000 and beyond. Am. Sci. **85**(4), 324–337 (1997)
22 Harik, W.M.: Ranges of applicability for the continuum-beam model in the constitutive analysis of carbon-nanotubes and nanorods. Solid State Commun. **120**, 331–335 (2001)
23 Wang, C.Y., Ru, C.Q., Mioduchowski, A.: Applicability and limitations of simplified elastic shell equations for carbon nanotubes. ASME J. Appl. Mech. **71**, 622–631 (2004)
24 Peng, J., Wu, J., Hwang, K.C., et al.: Can a single-wall carbon nanotube be modeled as a thin shell? J. Mech. Phys. Solids **56**, 2213–2224 (2008)
25 Han, Q., Lu, G.X., Dai, L.M.: Bending instability of an embedded double-walled carbon nanotube based on Winkler and van der Waals models. Compos. Sci. Technol. **65**, 1337–1346 (2005)
26 Shen, H.S., Zhang, C.L.: Postbuckling of double-walled carbon nanotubes with temperature dependent properties and initial defects under combined axial and radial mechanical loads. Int. J. Solids Struct. **44**, 1461–1487 (2007)
27 Sun, C., Liu, K.: Combined torsional buckling of multi-walled carbon nanotubes coupling with radial pressures. J. Phys. D: Appl. Phys. **40**, 4027–4033 (2007)
28 Saito, R., Matsuo, R., Kimura, T., et al.: Anomalous potential barrier of double-wall carbon nanotube. Chem. Phys. Lett. **348**, 187–193 (2001)
29 Timoshenko, S.P., Gere, J.M.: Theory of Elastic Stability in Chinese. Science Press, Beijing (1965)